PHYSICAL REVIEW A VOLUME 42, NUMBER 10 15 NOVEMBER 1990

Large-scale elastic-plastic indentation simulations via nonequilibrium molecular dynamics

William G. Hoover
Department of Physics, Keio University, Yagami Campus, Yokohama 223, Japan
*and Department of Applied Science, University of California at Davis-Livermore, Livermore, California 94550**

Anthony J. De Groot
Engineering Research Division, Lawrence Livermore National Laboratory, Livermore, California 94550

Carol G. Hoover
Department of Physics, Keio University, Yagami Campus, Yokohama 223, Japan
*and National Energy Supercomputer Center, Lawrence Livermore National Laboratory, Livermore, California 94550**

Irving F. Stowers
Precision Engineering Program, Lawrence Livermore National Laboratory, Livermore, California 94550

Toshio Kawai
Department of Physics, Keio University, Yagami Campus, Yokohama 223, Japan

Brad Lee Holian
Theoretical Division, Los Alamos National Laboratory, Los Alamos, New Mexico 87545

Taisuke Boku
Department of Computer Science, Keio University, Yagami Campus, Yokohama 223, Japan

Sigeo Ihara
Hitachi Central Research Laboratory, Kokubunji, Tokyo 185, Japan

J. Belak
Lawrence Livermore National Laboratory, Livermore, California 94550

(Received 14 June 1990)

Nonequilibrium indentation simulations for two-dimensional crystals composed of up to $1\,036\,800 = 720 \times 1440$ atoms are described. The forces used include smoothly truncated Lennard-Jones force laws, both with and without added embedded-atom contributions typical of copper or nickel. Both low and intermediate temperatures are considered over a wide range of indentor speeds. Typical microhardness yield strengths for these two-dimensional materials, force divided by projected area, exceed 10% of the shear modulus. For the most part these simulations were carried out on the 64-transputer SPRINT computer at Livermore.

I. INTRODUCTION

Molecular dynamics is now a mature field[1,2] and a flourishing worldwide enterprise.[3] The subject began with Fermi, Pasta, and Ulam's dynamical studies of one-dimensional anharmonic chains, Alder and Wainwright's detailed hard-sphere studies, and Vineyard's crude simulations of radiation damage in metals. In those days, between 30 and 40 years ago, 1000 atoms was a very large system. Today, with low-cost transputer technology and parallel processing,[4-6] million-atom simulations are feasible on a college or university budget. *Billion*-atom simulations are on the near horizon. Such large-scale simulations make it possible to model the dynamical behavior of micrometer-sized samples of real materials on an atomistic basis.

Million-atom simulations are already large enough to be of use in understanding applied problems in nanometer processing technology. The real challenge today is the accurate shaping of contoured surfaces on a scale of nanometers. State-of-the-art precision machining has progressed from relative accuracies of 10^{-6} m (1930), to 10^{-7} m (1948), to 10^{-8} m (1970), to today's ultimate limit of nanometer technology[7] in just 60 years. Today it is possible to machine precise contours with a depth of cut of only two or three atomic spacings. More typically, contour accuracies of a nanometer are achieved with cut depths of order 1 μm. Because such atomic-scale processing is slow, with production rates measured in square meters per year, the incentives for understanding are economic as well as intellectual. Simulating such processes is becoming a reality as the length scales of atomis-

©1990 The American Physical Society

tic simulations and laboratory measurements overlap[8,9] over an increasingly wider range of length scales. Atomistic simulations require a phenomenological description of atomistic interactions. The relative expense of three-dimensional simulations and the difficulties in visualizing the results make it mandatory first to carry out thorough exploratory two-dimensional studies. Two-dimensional studies are described in this paper. The present work is a substantial step toward the near future of molecular simulations, three-dimensional simulations involving *billions* of atoms.

It has long been understood that dynamical simulations, as opposed to arbitrary Monte Carlo selection rules, are essential to understanding nonequilibrium systems.[10] Previous dynamical work on simulating the nonequilibrium deformation of "simple metals," such as copper, dates back to Vineyard's radiation-damage studies at the Brookhaven Laboratory. There is no shortage of papers[11–14] discussing the qualitative simulation of material failure but comprehensive *quantitative* agreement with experiment on the basis of a fundamentally sound model has not yet been achieved. The theoretical world of one-electron atoms and dislocations governed by linear elastic forces bears little resemblance to engineering practice. Nearly ten years ago we began to study the steady plastic flow of solids at high rates of strain.[15,16] These studies emphasized isothermal plane Couette flow. Extrapolating from computer-generated flows at terahertz and gigahertz strain rates to reach "high-strain-rate" laboratory data at megahertz strain rates suggested overall agreement with the steady shear stress varying as a temperature-dependent power of the strain rate. Similar investigations have been carried out since that time, but without a systematic investigation of rate dependence, size dependence, force-law dependence, and temperature dependence. The transputer technology available today provides a qualitative change in the tools available for solving state-of-the-art problems in computational physics. Because engineering practice has reached the atomic scale this is an appropriate time for a reinvestigation of the fundamentals of material failure at relatively high strain rates and on relatively small scales.

In the past decade new simple models for interatomic interactions have been developed, greatly improving our capability for representing the nonadditive properties of metals. Pair potentials cannot describe metals. There is typically a severalfold disparity between the energy binding a single metal atom to a crystal and the energy associated with a vacant lattice site. Likewise, the disparity between the two elastic constants $C_{1122} \equiv C_{12}$ and $C_{1212} \equiv C_{44}$ in cubic crystals can only be reproduced by phenomenological models incorporating nonpair interactions. The "embedded-atom" concept invented by Foiles, Baskes, and Daw,[17] provides simple, inexpensive, and flexible many-body potentials to model at least some of the nonadditive properties of relatively simple metals without the computational complexity of explicit angle-dependent or long-ranged Coulomb forces. This enhanced capacity for realism, coupled with the still-rapidly-increasing size of simulations, promises revolutionary gains in understanding processes fundamental to metal cutting and deformation. The main outstanding gap is a simple flexible model consistent with the high strength of body-centered-cubic materials such as iron and tungsten.

We present here results from our two-dimensional study of indentation from an atomistic viewpoint. We characterize the dependence of indentation microhardness on force law, size, indentation rate, and temperature. We believe that such a systematic study is much more useful than isolated special simulations designed to model some aspect of single experiments. Indentation was selected here as the simplest fundamental measure of irreversible plastic yielding. The extension of these simulations to three-dimensional billion-atom cutting and polishing processes requires the efficient manipulation and analysis of large data files. We expect to contribute to this capability by laying a groundwork in two dimensions where the observed phenomena and the corresponding analyses are considerably simpler.

The plan of the present work includes an outline of the problem, in Sec. II; a description of the atomistic models, in Sec. III; a description of the computational implementation, in Sec. IV; with the results and conclusions derived therefrom making up Secs. V and VI.

II. INDENTATION

The behavior of linearly elastic materials follows Hooke's law,[18] with the stress proportional to the strain: $\sigma_{ij} = \sum C_{ijkl}\epsilon_{kl}$, or, in a more-abbreviated notation, $\sigma = C:\epsilon$. In three dimensions stress and strain are symmetric second-rank tensors with six independent components. In two dimensions the corresponding tensors have just three independent components, *xx*, *xy*, and *yy*. The proportionality constants making up the fourth-rank tensor C are the "elastic constants" and can range over about seven orders of magnitude, from the shear modulus of rubber, about 1 bar, to the longitudinal modulus of diamond, about 10 Mbar. Nonlinearly elastic materials follow a reversible stress-strain relation $\sigma = \sigma(\epsilon)$ without the hysteresis and irreversible heating associated with plastic yielding and permanent deformation.

It is usual, in continuum mechanics, to distinguish between rate-dependent "viscous" or "viscoelastic" flows and rate-*independent* "elastic" or "plastic" flows. These are useful idealizations for distinguishing the flow properties of brittle and ductile materials and reflect traditional engineering tests measuring the elastic moduli and the plastic yield strength. Idealized elastic and plastic behavior is illustrated in Fig. 1 for the inelastic elongation of a bar. The initial *elastic* response is described by Young's modulus, $\sigma_{xx}/\epsilon_{xx}$. Typically, at strains of order 0.001, the linear behavior changes, and the bar suffers "*plastic* strain," retaining a permanent deformation when the load is removed. Such plastic deformation is *irreversible* in a thermodynamic sense, and is characterized by the conversion of work to heat as well as by strain-induced hardening. Although permanent deformation is fundamentally dependent on both rate and temperature, the idealization of a constant yield strength, independent of strain and strain rate, is a useful conceptual and compu-

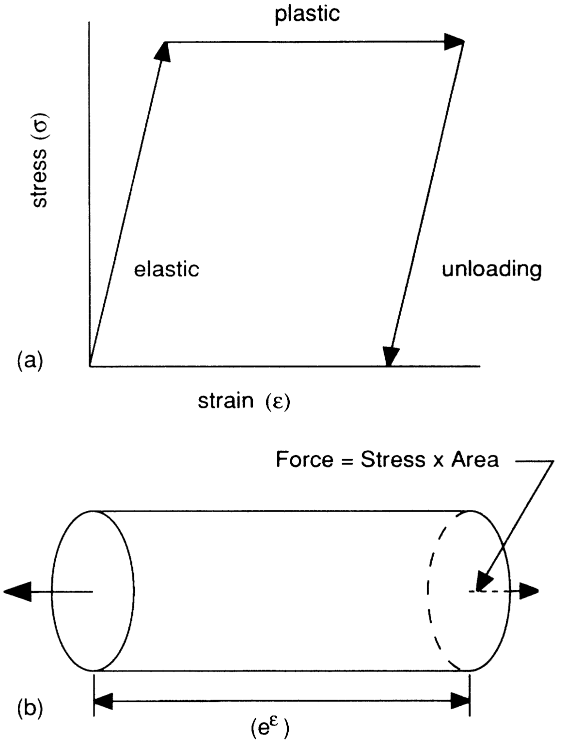

FIG. 1. Idealized elastic and plastic variation of stress σ_{xx} with strain ϵ_{xx} in the measurement of Young's modulus $\sigma_{xx}/\epsilon_{xx}$ and Poisson's ratio $-\epsilon_{yy}/\epsilon_{xx}$ by extending a cylindrical rod. The unloaded residual strain, relative to the original rod length, indicates plastic deformation.

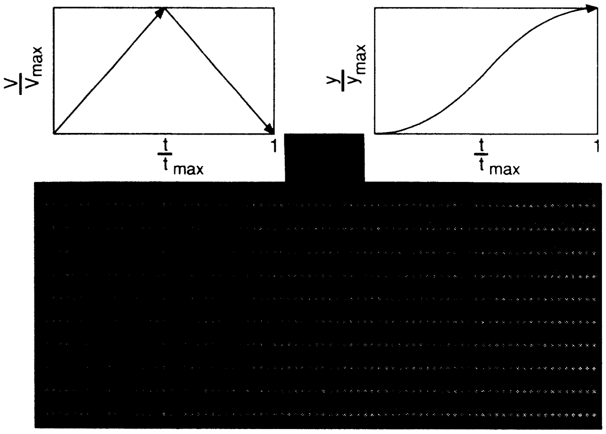

FIG. 2. Typical indentation geometry, shown here for a $3200=80\times40$ atom workpiece. The indentor radius is $4d$ where d is the cold-crystal interparticle spacing. The bottom row of atoms is fixed and the left and right boundaries of the workpiece are joined with periodic boundaries. The time-dependent indentor speed and displacement are shown in the insets.

tational model. We keep this simple model in mind while studying the more complicated phenomena associated with indentation.

When a macroscopic prismatic indentor is pressed into a mass of material, the resulting area of deformation is proportional to the applied load. The load per unit projected area is a phenomenological yield stress or "microhardness." For such a measure of yield we use the symbol Y. In our exploratory two-dimensional simulations Y is a *load per unit length* rather than a load per unit area. Our indentation geometry is shown in Fig. 2. We chose a circular, rather than triangular, indentor shape in an effort to simplify our results by minimizing singular stress gradients in the vicinity of the indentor tip. The indentor diameter was chosen to be a factor of 10 less than the zero-temperature system width in order to reduce the influence of the boundary image forces on the energy. Our two-dimensional circular indentor would correspond, in three dimensions, to pressing a cylindrical indentor into a half space of test material. The continuum description of such a deformation corresponds either to a problem in "plane strain," with no *displacements* in the direction normal to the picture plane of Fig. 2, or to a problem in "plane stress," with no *forces* in the direction normal to the picture plane.

Timoshenko and Goodier[18] describe the linearly elastic deformation of a two-dimensional isotropic half space by a point load. Despite displacements that diverge, logarithmically, at both small and large r, the stress field for this problem is well behaved. The solution shows that both the mean stress and the shear stress are proportional to the applied load and fall off as $\cos(\theta)/r$, where the direction of indentor travel defines the line $\theta=0$. The contours of equal shear stress are circles, as shown in Fig. 3. In the quasistatic plastic case, the shear stress cannot exceed the yield value Y. Thus the stress should closely follow the elastic solution outside a roughly circular contour about equal to the indentor in size and corresponding to the yield-zone boundary. Within the plastic zone the shear stress should be relatively constant and approximately equal to the microhardness Y. The linearly elastic solution for the geometry we have chosen, with periodic vertical boundaries and a rigid boundary at the workpiece base, can be very nearly described by a superposition of the half-space solutions, equally spaced in the horizontal direction, satisfying the periodic boundaries, and with a set of "image-load" solutions symmetrically

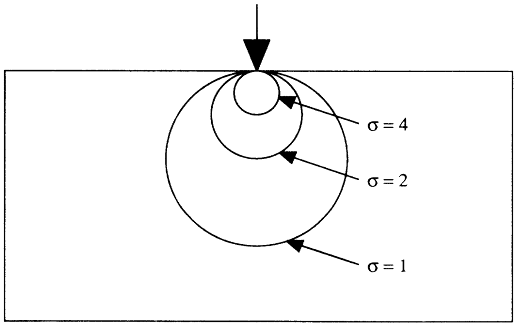

FIG. 3. Contours of equal stress, either compressive $[-(\sigma_{xx}+\sigma_{yy})/2]$ or shear $[(\sigma_{xx}-\sigma_{yy})^2/4+\sigma_{xy}^2]^{1/2}$, for a point load applied to an elastic half space in plane stress or plane strain, from Ref. 18.

arranged below the workpiece base, satisfying the rigid boundary conditions. The analytic elastic solution serves as a useful overall guide to choosing the workpiece shape and dimensions. A quantitative description, including irreversible plastic deformation, requires exploring many-parameter numerical solutions of the corresponding continuum dynamical equations, with both nonlinear elasticity and rate-dependent plasticity. Such numerical work is currently underway.[19]

The simplest continuum models of material behavior are rate independent. An "elastic" continuum responds to strain with a definite stress. In the elastic case there is no explicit dependence of stress on the rate of deformation. A "plastic" continuum *flows* irreversibly in response to a sufficiently large shear stress, so that stress and strain are no longer linked by a one-to-one reversible constitutive relation. But still, in the simplest case of rate-independent plasticity, there is no explicit dependence of the stress-strain relation on strain rate. According to either of these simple continuum models, elastic or plastic, or even a combination, there can be no "size effect;" that is, a small-size model of a large-size experiment should deform in exactly the same way, with the same stresses and strains, provided that these mechanical variables are functions of the scaled coordinates $\{x_s,y_s\}=\{x/L,y/L\}$. The predicted dependence of the energy of deformation on the scale length L is quadratic, in two dimensions. To see this scaling argument in more detail, take the equation of motion,

$$\rho\frac{d^2r}{dt^2}=\rho\frac{du}{dt}=\nabla\cdot\sigma(\epsilon)\ ,$$

and introduce dimensionless "scaled" coordinates $(r_s\equiv r/L)$ and a dimensionless scaled time $t_s\equiv ct/L$. Both the sound speed c and the density ρ are characteristic material properties which do not vary with the scale. If we multiply the equation of motion by L and then express the result in terms of these new variables, including the scaled velocity $u_s\equiv dr_s/dt_s$ and the scaled gradient $\nabla_s\equiv L\nabla$ we have

$$L\left[\rho\frac{du}{dt}\right]=L\left[\rho\frac{d(cu_s)}{d(Lt_s/c)}\right]=\rho c^2\frac{du_s}{dt_s}=L[\nabla\cdot\sigma(\epsilon)]$$
$$=\nabla_s\cdot\sigma(\epsilon)\ ,$$

establishing that the equation of motion, and hence its solution, is *scale-independent*. The only necessary assumptions are that the stress is a definite function of strain and that the set of boundary Mach numbers, $\{v/c\}$ for any moving boundaries, is scale independent.

The simplest atomistic view suggests a different conclusion, based on the idea that plastic flow is the result of dislocation motion so that the resulting strain *rate* is a function of stress. This viscoelastic viewpoint is consistent with studies of dislocation motion carried out over a wide range of temperatures and system sizes, both in two and in three dimensions.[15] From the atomistic viewpoint dislocations move at speeds of the order of the transverse sound speed in acting to reduce the shear stress. This viewpoint suggests an Arrhenius (exponential) relation between flow rate and inverse temperature with enhanced strength for smaller samples and higher rates of deformation. In this paper we describe our efforts to compare the results of direct numerical simulation with these simple models.

III. ATOMISTIC DYNAMICS

We consider regular close-packed "triangular-lattice" crystals in which all pairs of particles interact with the short-ranged Lennard-Jones spline potential,[20] which very smoothly connects the Lennard-Jones 6-12 potential to a cubic spline between the potential's inflection point R_i and a cutoff R_m at 1.547 537 times the potential's rest-length d:

$$\phi_{\mathrm{LJS}}(r)=\epsilon[(d/r)^{12}-2(d/r)^6]\quad\text{for } r<R_i\ ,$$

$$\phi_{\mathrm{LJS}}(r)=4.655\,595(\epsilon/d^3)(R_m-r)^3$$
$$-6.129\,377(\epsilon/d^2)(R_m-r)^2\quad\text{for } R_i<r<R_m\ .$$

$$R_i/d=(13/7)^{1/6}=1.108\,683,\quad R_m/d=1.547\,537\ .$$

The three constants in the spline potential follow from matching the values of the potential and its first two derivatives at the inflection point R_i.

We also include similar calculations using an embedded-atom collective potential.[17] We use the Holian-Voter-Hoover embedded-atom potential. The goal was to model the vacancy energy and elastic properties of a simple metal such as copper or nickel with as simple a functional form as possible. We chose to write the additional energy as a sum, over all atoms, of a density-dependent potential $\phi_{\mathrm{EA}}(\rho)$:

$$\Phi_{\mathrm{EA}}=\sum\phi_{\mathrm{EA}}(\rho)=2\epsilon e\sum_i(\rho_i\ln\rho_i)\ ,$$

$$\rho_i=\sum_j\rho_{ij}\ ,$$

$$\rho_{ij}=(1/6e)[(R_m^2-r^2)/(R_m^2-d^2)]^2\ ,$$

where the individual-particle densities $\{\rho_i\}$ are computed as sums of the short-ranged quartic function which vanishes at the potential cutoff distance R_m. In the perfect-lattice arrangement a particle with six neighbors has an embedding density of $1/e$, at which the energy is minimized, corresponding to a negative binding energy of -2ϵ per particle. In this present work we match the energy minima for the two potentials by adding onto Φ_{EA} the usual Lennard-Jones-spline potential, multiplied by $\frac{1}{3}$, so that the perfect-crystal energies for the Lennard-Jones and Lennard-Jones plus embedded-atom models are identical, -3ϵ per particle. The embedded-atom potential acts to drastically reduce the crystal vacancy energy. If a single vacancy is introduced into a stress-free static Lennard-Jones crystal the energy change is $+3\epsilon$, exactly the same as the binding energy per particle. In the embedded-atom case moving an atom within the crystal so as to create a vacancy causes the density of the six atoms neighboring the vacancy location to change from $1/e$ to $5/6e$. The corresponding change in the embedded-atom contribution to the total crystal energy

$\Phi_{\rm EA}$ is $\epsilon[10\ln(5/6e)-12\ln(1/e)]=+0.177\epsilon$, less than one-tenth the embedded-atom binding energy per particle.

The change in the elastic properties is dramatic too because *the embedded-atom contribution to the zero-temperature zero-pressure shear modulus is exactly zero.* For the regular triangular-lattice arrangement the change in embedding density is *quadratic* in the shear strain rather than linear so that the linear-elastic embedded-atom resistance to shear vanishes. As a result the two potentials have *different* zero-pressure melting temperatures (about $0.40\epsilon/k$ for the Lennard-Jones-spline potential and $0.20\epsilon/k$ for the Lennard-Jones plus embedded-atom potential) and different elastic properties. The factor-of-2 drop in the melting temperature corresponds roughly to the drop in lattice frequencies of those modes resisting shear. The reduction is exactly a factor $\sqrt{3}$, reflecting the factor-of-3 decrease in the Lennard-Jones contribution in the Lennard-Jones plus embedded-atom potential. It is possible to match the bulk modulus, as well as the binding energy, by using a Morse potential developed by Holian, rather than the Lennard-Jones-spline potential, but we have not investigated that somewhat softer potential here.

In describing the elastic properties of solids the Lamé-constant description is a useful one because the triangular-lattice structure implies elastic isotropicity. In the plane-strain interpretation of our two-dimensional results the elastic constitutive equations have the forms

$$\sigma=\lambda\nabla\cdot uI+\eta(\nabla u+\nabla u^t)\ ,$$

$$\sigma_{xx}=(\lambda+2\eta)\epsilon_{xx}+\lambda\epsilon_{yy}\ ,\quad \sigma_{xy}=\eta\epsilon_{xy}\ ,$$

$$\sigma_{yy}=\lambda\epsilon_{xx}+(\lambda+2\eta)\epsilon_{yy}\ ,$$

where the elastic displacement relative to the stress-free configuration is the vector $u=(u_x,u_y)$ and I is the unit tensor. *With central forces* the zero-temperature zero-pressure shear modulus G, and the two Lamé constants, η and λ, are all three equal for any two-dimensional triangular-lattice system. We can estimate these moduli from the equation of state of the cold crystal. For the pure Lennard-Jones-spline force law these relations are

$$PV/N\epsilon=18(\rho/\rho_0)^6-18(\rho/\rho_0)^3\ ,$$

$$BV/N\epsilon=2GV/N\epsilon=126(\rho/\rho_0)^6-72(\rho/\rho_0)^3\ ,$$

where ρ_0 is the two-dimensional zero-temperature stress-free density, $\rho_0=(4/3)^{1/2}(m/d^2)$. P and V indicate the equilibrium pressure and volume for an N-atom crystal. B is the zero-temperature bulk modulus, $-V(dP/dV)_0$. Thus, for the cold stress-free lattice:

$$\begin{aligned}BV/N\epsilon&=(\lambda+\eta)V/N\epsilon=2GV/N\epsilon\\&=2\eta V/N\epsilon=54\quad\text{(LJS)}\ .\end{aligned}$$

These contributions are reduced threefold in the Lennard-Jones plus embedded-atom case. The corresponding pure embedded-atom contribution to the bulk modulus $B=\lambda+\eta$ is $4.1N\epsilon/V$, leading to the additional zero-temperature stress-free results:

$$BV/N\epsilon=(\lambda+\eta)V/N\epsilon=22.1\ ,$$

$$\lambda V/N\epsilon=13.1\ ,$$

$$GV/N\epsilon=\eta V/N\epsilon=9\quad\text{(LJEA)}\ .$$

These elastic constants are useful in comparing the results of our atomistic simulations with the predictions of continuum mechanics and with experimental findings, as is briefly discussed in Sec. V. Preliminary qualitative investigations[21] showed a good correspondence with elastic theory. We expect to present more detailed comparisons[19] with numerical continuum plasticity simulations in the near future.

It has been emphasized[6] that centered-difference "modified-Stoermer" methods generalizing Verlet's equilibrium approach to nonequilibrium simulations are both stable and useful for relatively large time steps, $dt=0.02(md^2/\epsilon)^{1/2}$ for the Lennard-Jones-spline calculations and $dt=0.03(md^2/\epsilon)^{1/2}$ for the slightly softer embedded-atom simulations, and also require minimum storage. Accordingly we have used the Stoermer form:

$$x_+-2x_0+x_-=(dt)^2(F_0/m)\ ,$$

for our cold-crystal simulations. At nonzero temperatures a very powerful and flexible type of temperature control can be applied by using a modified-Stoermer generalization of Nosé-Hoover mechanics.[6] In general, individual thermostat temperatures T_j and relaxation times τ_j can be imposed on selected subsets $\{x_i\}$ of the system degrees of freedom by "friction coefficients" ζ_j. The corresponding equations of motion for the members of such a subset can include a space-and-time dependent weighting function $w_j(x_i,t)$:

$$\frac{d^2x_i}{dt^2}=(F_i/m_i)-w_j(x_i,t)\zeta_j\frac{dx_i}{dt}\ ,$$

$$\frac{d\zeta_j}{dt}=w_j(x_i,t)[(p_i^2/m_ikT_j)-1]/\tau_j^2\ .$$

We call ζ a "friction coefficient" in order to suggest an analogy with the functional form of hydrodynamic drag forces. The present friction coefficients have no direct relation or connection to real macroscopic friction and appear in the (time-reversible) equations as temperature-control variables. It is not difficult to show that in the equilibrium case, where the imposed temperatures $\{T_j\}$ have a common value, T, these Nosé-Hoover equations of motion preserve Gibbs's canonical-ensemble phase-space distribution for an otherwise isolated system. Thus the friction coefficients are the deterministic mechanical equivalent of a thermodynamic heat bath. For simplicity, in our finite-temperature indentation simulations we apply a *uniformly* weighted thermostat, with no explicit space or time dependence, to *all* degrees of freedom. The time-reversible finite-difference equations, with which we approximate the solution of the differential equations of motion given above, are these:

$$x_+ - 2x_0 + x_- = (dt)^2(F_0/m) - \zeta_0(x_+ - x_-)(dt/2) ,$$

$$\zeta_+ - \zeta_- = [(K_0/NkT) - 1](2dt)/\tau^2 ,$$

$$K_0 = (1/dt)^2 \sum (m/8)(x_+ - x_-)^2 .$$

The subscripts $\{-,0,+\}$ indicate successive times separated by the time step dt. New coordinates, "+," are first calculated using the current value "0" of the friction coefficient, ζ_0; then the new value of the friction coefficient, ζ_+, can be calculated from the kinetic energy K_0 based on these new coordinates $\{x_+\}$. The long-time average value of the kinetic energy is NkT where T is the temperature and N is the number of (moving) particles (excluding the bottom row of fixed particles). The arbitrary relaxation time τ is set equal to $(md^2/\epsilon)^{1/2}$ except at the higher rates of deformation, for which $\tau = 0.1(md^2/\epsilon)^{1/2}$.

IV. COMPUTATIONAL DETAILS

The calculations were made as simple as possible by using the short-ranged Lennard-Jones-spline potential. In our exploratory work on the CRAY computers at Livermore we constructed neighbor lists[22] for each particle. For the 64-megabyte SPRINT it was advantageous to save space, spanning the problem geometry by a network of rectangular cells, each of sidelength twice the mean nearest-neighbor spacing, and to keep track of each cell's occupants by using a linked list.[22] In this way the number of storage locations per atom was reduced to about nine, two coordinates at each of three times and an additional three locations per particle describing the distribution of particles among cells. At the expense of programming clarity it is possible to reduce the required storage by an additional two locations per particle[2] by introducing "velocities" described by a "leapfrog" version of the Stoermer algorithm. Again for simplicity all of our simulations were geometrically similar, with m horizontal rows of $2m$ particles each making up the workpiece, as

TABLE I. The work of indentation, in units of ϵ, is tabulated for an indentor travel distance of $(Nd^2/200)^{1/2}$, where N is the number of particles. The force laws indicated are the Lennard-Jones-spline and the combination of that potential with an embedded-atom potential, as described in the text. For both these potentials "cold" indicates the adiabatic indentation of an initially static crystal and "hot" indicates the isothermal indentation of a crystal at half the melting temperature. [The melting temperatures are $0.40(\epsilon/k)$ for LJS and $0.20(\epsilon/k)$ for LJEA, respectively.] The *average* indentor speed, in units of $(\epsilon/m)^{1/2}$, is half the tabulated maximum value. See Fig. 2. The uncertainty in the results quoted is due primarily to the underlying chaotic dynamics. Comparisons of calculations with slightly different initial conditions suggest that this uncertainty is of the order of a few to several percent.

Number	Temperature	Maximum speed	*W*(LJS)	*W*(LJEA)
800	Cold	0.0010	51	17
800	Cold	0.0100	49	18
800	Cold	0.1000	48	19
800	Cold	1.0000	82	35
800	Hot	0.0001		7
800	Hot	0.0010	32	8
800	Hot	0.0100	40	12
800	Hot	0.1000	48	16
800	Hot	1.0000	62	26
3200	Cold	0.0010	172	59
3200	Cold	0.0100	183	67
3200	Cold	0.1000	224	72
3200	Cold	1.0000	292	121
3200	Hot	0.0010	127	59
3200	Hot	0.0100	127	57
3200	Hot	0.1000	165	56
3200	Hot	1.0000	233	124
12 800	Cold	0.0100	877	278
12 800	Cold	0.1000	890	321
12 800	Cold	1.0000	1115	418
12 800	Hot	0.0040	507	208
12 800	Hot	0.0100	516	219
12 800	Hot	0.1000	587	241
12 800	Hot	1.0000	805	401
1 036 800	Hot	1.0000	41 300	22 200

was shown in Fig. 2. The bottom row of particles was held fixed and periodic boundaries were applied at the ends of the rows. Simulations were carried out for cold crystals, with the minimum-energy nearest-neighbor spacing d, and at temperatures half the melting temperature, $kT/\epsilon=0.20$ for the Lennard-Jones-spline potential and 0.10 for the Lennard-Jones plus embedded-atom potential. At these temperatures the nearest-neighbor spacing was increased to correspond to the stress-free value. The required increases were 2.25% (LJS) and 2.5% (LJEA).

In all of our simulations the total indentor displacement was set equal to the indentor radius and the indentor speed was a continuous function of time. See Fig. 2 and Table I. At zero temperature the longitudinal sound speed in the two-dimensional Lennard-Jones-spline material is $9(\epsilon/m)^{1/2}$. We accordingly chose loading schedules in which the maximum indentor speed never exceeded $(\epsilon/m)^{1/2}$. The time-dependence of the indentor velocity, as well as the corresponding indentor displacement, are shown as insets, in Fig. 2. We found that relatively slow maximum speeds, of order $0.01(\epsilon/m)^{1/2}$, were required to obtain quasistatic results.[21]

The interactions between all of the particles were exactly the same, but the interactions between particles and the indentor were taken as the repulsive part of the Lennard-Jones potential. We checked to verify that our results were insensitive to this choice.

V. RESULTS

In our exploratory work we found that sequences of pictures, particularly videotapes, were essential to a qualitative understanding of the indentation process. The low-temperature movies of elastically deforming crystals show motions with a strong visual resemblance to quivering Jello. Dislocations advance and retreat many times, and over different paths, before the final permanent deformation mode stabilizes. Figure 4 shows a particularly interesting low-temperature final configuration in which a wedge of material below the indentor has penetrated one lattice spacing into otherwise defect-free material. This deformation strongly resembles a plastic slip-line solution. The movies also show a marked temperature dependence of yield morphology with widespread flow at half the melting temperature and considerable, relatively rapid diffusion of surface atoms.

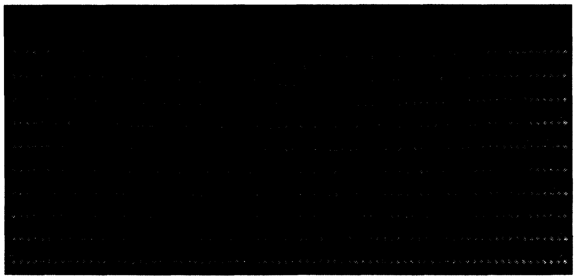

FIG. 4. Final configuration of a 3200-atom cold Lennard-Jones crystal. The displaced wedge of material under the indentor has been made visible by using a repeating sequence of four colors to indicate the displacements of the originally horizontal rows of atoms.

The fundamental measured quantity in all of our simulations is the time history of the work of indentation W_I:

$$W_I=\int dW_I=\int F_I dy=\int F_I \frac{dy}{dt}\,dt>0\ .$$

F_I is the vertical component of the force exerted on the workpiece by the indentor. An independent estimate of the indentation work follows from energy conservation, $W_I=-\Delta W=\Delta E-\Delta Q$, where ΔE is the change in system energy during indentation, including the potential energy of interaction with the indentor, and $-\Delta Q$ is the heat extracted from the system by the thermostatting forces. From the continuum standpoint the indentor force can be viewed as the product of a phenomenological yield stress or microhardness [with units (energy)/(length)^D in D dimensions] and the corresponding projected area ($D=3$) or length ($D=2$) to which the stress is applied. In two dimensions the resulting total work of indentation is given by the integral

$$W_I=\int 2Y(R^2-h^2)^{1/2}dh=YR^2\int 2\cos^2(\theta)d\theta$$
$$=Y\pi R^2/2\ ,$$

where h is the height of the indentor's center above the horizontal workpiece surface. Thus the yield stress is approximately equal to the work done per unit area of indentation. In three dimensions the corresponding yield stress is the work per unit volume, with the indentation volume equal to half the cylindrical indentor volume $(\pi/2)R^2L$, with the indentor length L assumed large relative to R.

The time history of the indentor force is plotted in Fig. 5 for a workpiece with more than a million atoms. The *decrease* in indentor force, closely following the decrease in indentor speed, indicates that the response is *dissipative* rather than elastic. Further, the late-time absolute decrease in the magnitude of force as a function of displacement shows that the response must be at least partially viscoplastic or strain-softening, for the contact area increases monotonically. A portion of a typical configuration of this same simulation is shown in Fig. 6. Note the dislocations and voids formed directly below the indentor as well as the lack of overall symmetry between the left and right sides of the indentation cavity.

The results for small and large systems are similar, with somewhat larger relative fluctuations and with nearly discontinuous changes in indentor force reflecting structural changes. In two dimensions the smallest size sample for which we found useful results was composed of 800 atoms. The time history of the work of indenting a hot 800-atom embedded-atom crystal is plotted in Fig. 7. There are two well-defined changes of overall slope in the integrated work for this relatively small system.

To interpret our results we adopt the simple yield model discussed above. We imagine that the net vertical indentor force is the product of the yield strength Y and a perpendicular line segment against which the indentor force is applied, the work done is a direct measure of the

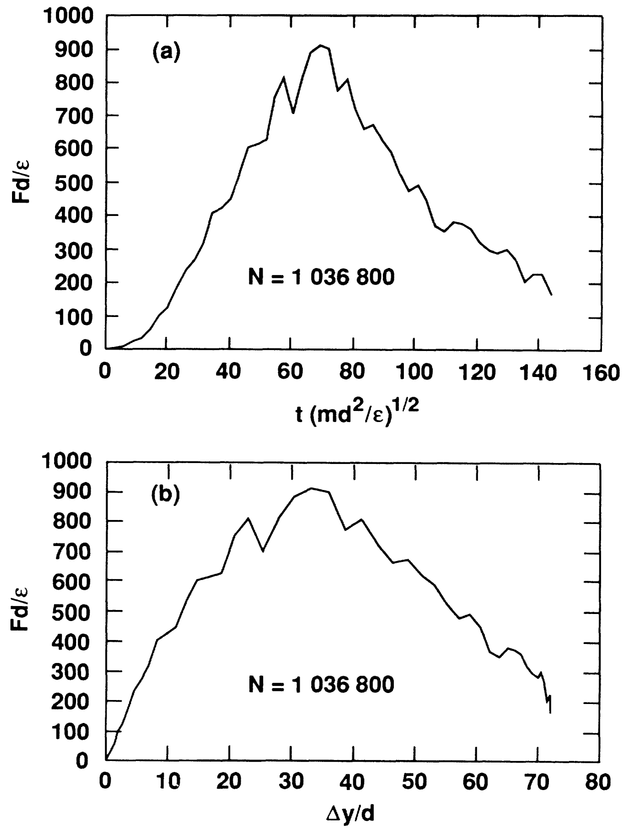

FIG. 5. Indentor force as a function of time and displacement for the indentation of 1 036 800 Lennard-Jones-spline particles at half the melting temperature. The force variation for smaller crystals is quite similar, but with larger fluctuations.

yield strength Y and equal to the microhardness. The raw results are complicated somewhat by their dependence on the scaled indentor velocity, v/c, as well as on the indentor size R. The dependence of stress on strain rate is evidently not a simple power law of the type found in Ref. 15 and 16. We attribute this difference in rate dependence to the inhomogeneity of the present strain field. If we use our lowest-speed energies as estimates for the work of *quasistatic* indentation the resulting estimates for the yield strength, $Y \equiv W_I/R^2$, give consistent results for both temperatures and both force laws. The ratio of the cold yield strength to the shear modulus is about $\frac{1}{4}$, slightly more for the stiffer Lennard-Jones crystal and slightly less for the metallic embedded-atom model. At half the melting temperature there is a reduction in strength of about 30% in both cases. The magnitude of the kinetic correction, for an indentor speed of order $(\epsilon/m)^{1/2}$, varies closely with R^2, as the view of indentation as slow-speed impact would suggest. At the reasonably slow speed of $0.001(\epsilon/m)^{1/2}$, the indentation process takes place over about 1000 sample sound traversal times, adequately slow for quasistatic compression.

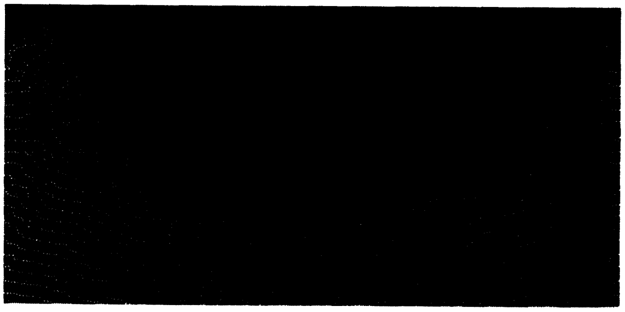

FIG. 6. Portion of a typical configuration of the 1 036 800-atom Lennard-Jones-spline simulation showing damage below the indentor and the lack of right-left symmetry in the indentation cavity.

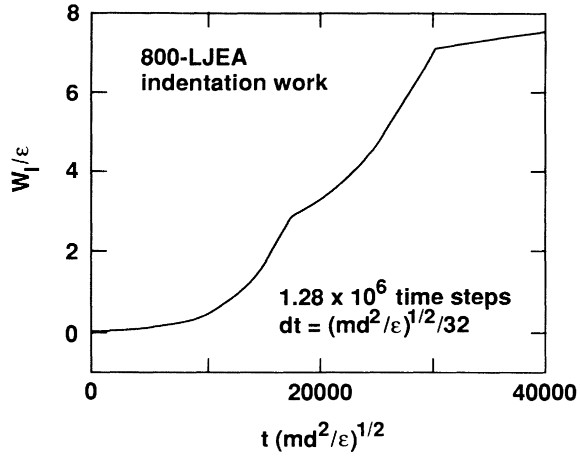

FIG. 7. Work of indentation for an 800-atom Lennard-Jones plus embedded-atom crystal at half the melting temperature. The simulation time of over one million time steps, $40\,000(md^2/\epsilon)^{1/2}$, corresponds to about 20 000 sound traversal times.

Our estimated yield strengths for both the Lennard-Jones-spline and the Lennard-Jones-spline plus embedded-atom potentials are plotted in Fig. 8. The data indicate that at sufficiently low rates *yield stress depends mainly on strain as opposed to strain rate.* Further, *the size effect appears to be small,* so small that simulations only 100 atomic diameters in width provide accurate estimates of large-system behavior. In this connection it is particularly satisfying to see the nice agreement among the scale-model yield estimates for indentor radii of 2*d*, 4*d*, 8*d*, and 72*d*. The data show that for indentor speeds exceeding 1% of the sound velocity definite kinetic effects increase the effective yield strength. The empirical yield strength is reduced by about 30% by heating the solid to half the melting temperature.

These results indicate first of all that the yield phenomenon in two-dimensional crystals at temperatures up to half the melting temperature differs qualitatively from the results of *macroscopic* hardness experiments on metals. There is a bewildering variety of experimental results, but it is fair to summarize these by stating that even the small micrometer-scale hardness values for pure metals are generally in the range from 0.05 to 5 gigapascals, that is, on the order of a percent of the shear modulus. On the other hand, some relatively old but careful experiments, carried out by Gane and Bowden[23] with a blunt indentor only slightly larger than that used in our

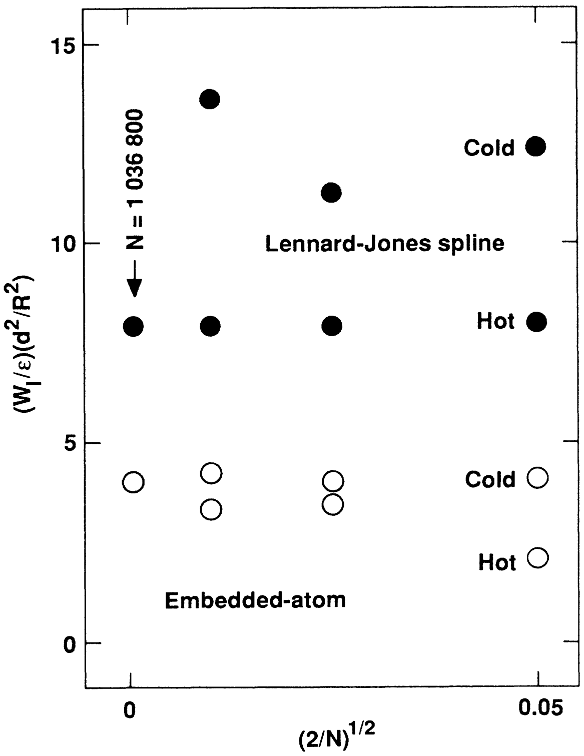

FIG. 8. Variation of the phenomenological yield strength, or "microhardness," $Y \equiv W_I/R^2$, with system size, temperature, and force law. This microhardness is the total work of indentation $-\int F_y dy$, divided by the square of the indentor radius. It is approximately equal to the applied load divided by the projected area. These microhardness values should be compared to the corresponding zero-temperature-and-pressure shear moduli, $27N\epsilon/V$ for the Lennard-Jones-spline potential, and $9N\epsilon/V$ for the Lennard-Jones plus embedded-atom potential.

million-atom simulations, showed a 30-fold increase in gold's microhardness. There is no reason to believe that our two-dimensional results would vary for larger scales. One might well expect that the accumulation of damage during an indentation or cutting process would provide sufficient defects for a realistic estimate of yield strength. We can only conclude that three-dimensional materials *may* actually be somewhat weaker than corresponding two-dimensional ones. This is possible because more slip directions are available for plastic flow in three dimensions than in two. The additional flow mechanisms might well reduce the yield strength by a factor of 10. Because we found no qualitative difference between the behavior of the Lennard-Jones and embedded-atom crystals we expect that the behavior of real materials can be adequately modeled by short-ranged forces of the types used in the present work.

We found that the computer time required for our (scalar) computer program increased by nearly a factor of 20 when the same program was executed on a CRAY2 computer. A different vector version, written for the 65 536-processor Connection Machine[24] at Los Alamos, was executed both on a CRAY-YMP and the Connection Machine. The YMP vector program was perhaps ten times faster than the CRAY2 scalar program, but still somewhat slower than SPRINT and restricted to system sizes of less than half a million atoms. The Connection Machine and the SPRINT have very similar speeds when applied to the problem. From the economic standpoint the SPRINT is superior to the much more costly supercomputers and to the Connection Machine. Our comparisons show that the newly installed Butterfly Machine at Livermore is two times faster than SPRINT with 31 processors, and probably eight times faster than 126, but this speed advantage of the Butterfly Machine is attained at a 25- to 100-fold increase in cost. SPRINT uses FORTRAN and can equally well be used to treat two- and three-dimensional problems in atomistic and continuum mechanics and so is a very efficient role-model tool for solving a wide range of problems in computational physics.

We expect to check the dependence on dimensionality by carrying out a three-dimensional indentation simulation with a million-atom crystal using exactly the same embedded-atom function. Earlier simulations[15] of steady plastic flow in two- and three-dimensional plane Couette flow geometry showed no real dependence on dimensionality and a stronger dependence on rate than that found here.

VI. CONCLUSION

By using relatively inexpensive transputer technology it is now possible to simulate the motion of one million atoms using conventional molecular dynamics. Storage requirements can be minimized by using modifications of the centered-difference Stoermer algorithms.

In the atomistic simulations of plastic flow in two-dimensional plane strain reported here we find that both the Lennard-Jones-spline potential and a modified embedded-atom potential thought to describe interactions in simple metals both lead to broadly similar conclusions: the yield strength, or microhardness, for a two-dimensional triangular-lattice material is of the order of one quarter of the shear modulus. This result is unambiguous, and depends only weakly on forces, system size, temperature, and strain rate. We are making an effort to study the continuum version of this same problem numerically on the SPRINT and Butterfly Machines. It still remains to be seen whether or not three-dimensional simulations will yield the somewhat lower strengths seen experimentally. Three-dimensional simulations are possible, so that this question should be answered soon.

ACKNOWLEDGMENTS

W.G.H. thanks the Japan Society for the Promotion of Science for its support during a sabbatical leave at Keio University's Yagomi Campus. C.G.H. thanks the Lawrence Livermore National Laboratory for support during a research leave at Keio University. Professor Shuichi Nosé provided help with several of the computer systems used in this work. W.G.H., A.J.D., C.G.H., I.F.S., and J.B. thank the Department of Energy for support under Contract No. W-7405-Eng-48. B.L.H. thanks the Department of Energy for support under Contract No. W-7405-36.

[*] Permanent address.

[1] W. G. Hoover, *Molecular Dynamics* (Springer-Verlag, Berlin, 1986).

[2] M. P. Allen and D. J. Tildesley, *Computer Simulation of Liquids* (Clarendon, Oxford, 1987).

[3] See, for instance, *Molecular Dynamics Simulation of Statistics-Mechanical Systems,* Proceedings of the Enrico Fermi Summer School Course 97, edited by G. P. Ciccotti and W. G. Hoover (North-Holland, Amsterdam, 1986).

[4] A. J. De Groot, S. R. Parker, and E. M. Johansson, in *SVD and Signal Processing; Algorithms, Applications and Architectures,* edited by E. F. Deprettere (North-Holland, Amsterdam, 1988).

[5] T. Hoshino, *Pax Computer* (Addison-Wesley, New York, 1989).

[6] B. L. Holian, A. J. De Groot, W. G. Hoover, and C. G. Hoover, Phys. Rev. A **41**, 4552 (1990). See also the preliminary report by W. G. Hoover, A. J. De Groot, B. L. Holian, I. F. Stowers, and T. Kawai, in *Proceedings of the Third Workshop on Molecular Simulation, Kyoto, 1990* (Kyoto University, Kyoto, 1990), pp. 55 and 56.

[7] N. Taniguchi, Ann. CIRP **32**, 573 (1983).

[8] T. P. Beebe, Jr., T. E. Wilson, D. F. Ogletree, J. E. Katz, R. Balhorn, M. B. Salmeron, and W. J. Siekhaus, Science **243**, 370 (1989).

[9] D. M. Eigler and E. K. Schweizer, Nature (London) **344**, 525 (1990).

[10] M. Schneider, A. Rahman, and I. K. Schuller, Superlattices and Microstructures **7**, 39 (1990).

[11] J. Maddox, Nature (London) **334**, 561 (1988).

[12] M. W. Ribarsky and U. Landman, Phys. Rev. B **38**, 9522 (1988); U. Landman, W. D. Luedtke, N. A. Burnham, and R. J. Colton, Science **248**, 454 (1990).

[13] D. Deng, A. S. Argon, and S. Yip, Philos. Trans. R. Soc. London, Ser. A **329**, 549 (1989).

[14] R. G. Hoagland, M. S. Daw, S. M. Foiles, and M. I. Baskes, J. Mat. Res. **53**, 13 (1990).

[15] W. G. Hoover, A. J. C. Ladd, and B. Moran, Phys. Rev. Lett. **48**, 1818 (1982).

[16] A. J. C. Ladd and W. G. Hoover, Phys. Rev. B **28**, 1756 (1983).

[17] S. M. Foiles, M. I. Baskes, and M. S. Daw, Phys. Rev. B **33**, 7983 (1986).

[18] S. P. Timoshenko and J. N. Goodier, *Theory of Elasticity* (McGraw-Hill, New York, 1970).

[19] W. G. Hoover, C. G. Hoover, T. Kawai, and T. Boku (unpublished).

[20] B. L. Holian and D. J. Evans, J. Chem. Phys. **78**, 5147 (1983).

[21] W. G. Hoover, C. G. Hoover, A. J. De Groot, I. F. Stowers, and W.J. Siekhaus, Mat. Res. Soc. Symp. Proc. **140**, 119 (1989).

[22] J. J. Morales, L. G. Rull, and S. Toxvaerd, Comput. Phys. Commun. **56**, 129 (1989).

[23] N. Gane and F. P. Bowden, J. Appl. Phys. **39**, 1432 (1968).

[24] B. Bhoghosian, Comput. Phys. **4**, 1 (1990).

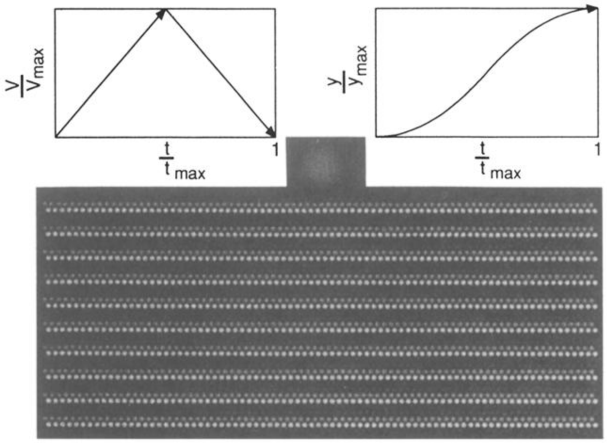

FIG. 2. Typical indentation geometry, shown here for a 3200 = 80 × 40 atom workpiece. The indentor radius is 4*d* where *d* is the cold-crystal interparticle spacing. The bottom row of atoms is fixed and the left and right boundaries of the workpiece are joined with periodic boundaries. The time-dependent indentor speed and displacement are shown in the insets.

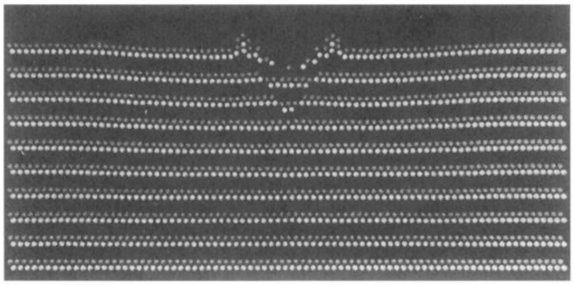

FIG. 4. Final configuration of a 3200-atom cold Lennard-Jones crystal. The displaced wedge of material under the indentor has been made visible by using a repeating sequence of four colors to indicate the displacements of the originally horizontal rows of atoms.

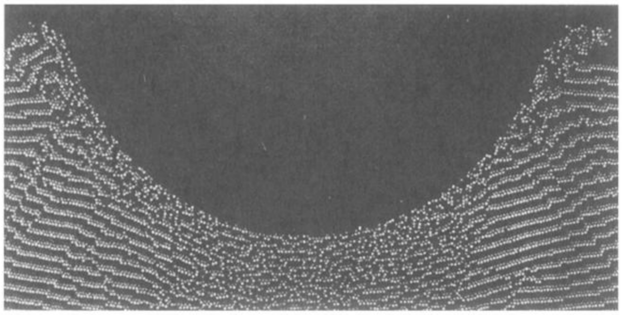

FIG. 6. Portion of a typical configuration of the 1 036 800-atom Lennard-Jones-spline simulation showing damage below the indentor and the lack of right-left symmetry in the indentation cavity.